Molecular Crystals and Liquid Crystals

ISSN: 1542-1406 (Print) 1563-5287 (Online) Journal homepage: http://www.tandfonline.com/loi/gmcl20

Synthesis, Crystal Growth, Characterization, and Theoretical Studies of 3-(4-fluorophenyl)-1-(4-methylphenyl)prop-2-en-1-one

V. Meenatchi, K. Muthu, M. Rajasekar & SP. Meenakshisundaram

To cite this article: V. Meenatchi, K. Muthu, M. Rajasekar & SP. Meenakshisundaram (2015) Synthesis, Crystal Growth, Characterization, and Theoretical Studies of 3-(4-fluorophenyl)-1-(4-methylphenyl)prop-2-en-1-one, Molecular Crystals and Liquid Crystals, 609:1, 171-182, DOI: 10.1080/15421406.2014.954309

To link to this article: http://dx.doi.org/10.1080/15421406.2014.954309

Mol. Cryst. Liq. Cryst., Vol. 609: pp. 171–182, 2015

ISSN: 1542-1406 print/1563-5287 online
DOI: 10.1080/15421406.2014.954309

Taylor & Francis
Taylor & Francis Group

Synthesis, Crystal Growth, Characterization, and Theoretical Studies of 3-(4-fluorophenyl) -1-(4-methylphenyl)prop-2-en-1-one

V. MEENATCHI, K. MUTHU, M. RAJASEKAR, AND SP. MEENAKSHISUNDARAM*

Department of Chemistry, Annamalai University, Annamalainagar, Tamilnadu, India

Single crystals of 3-(4-fluorophenyl)-1-(4-methylphenyl)prop-2-en-1-one (FMPP) have been grown by mixed solvent system ethanol and chloroform 2:1 (v/v) at room temperature. Single crystal X–ray diffraction reveals that FMPP belongs to monoclinic system with four molecules in the unit cell. The structure and the crystallinity of the material were further confirmed by FT-IR, FT-Raman, and powder X–ray diffraction analyses. The band gap energy is estimated by Kubelka–Munk algorithm using DRS data. Theoretical calculations were performed to derive the optimized geometry and the first-order molecular hyperpolarizability (β) values. The as-grown crystal is further characterized by GC-Mass, SEM, and thermal analyses.

Keywords FT-IR; hyperpolarizability; optical properties; thermal analysis; X–ray diffraction

1. Introduction

Chalcones and their derivatives are of high interest materials due to their antioxidant, antibacterial, antifungal, antitumor, and antiinflammatory properties [1–4]. The design and synthesis of organic molecules exhibiting second-order nonlinear optical (NLO) properties have been motivated by their tremendous potential for application in optical communications, optical computing, data storage, dynamic holography, harmonic generators, frequency mixing, and optical switching [5,6]. At the molecular level, compounds are likely to exhibit large values of molecular hyperpolarizability (β) and they must have polarizable electrons (e.g., π–electrons) spread over a large distance. It has been shown that extended π systems with terminal donor–acceptor substituents exhibit large β values [7,8]. Among many organic NLO materials, chalcone derivatives are noticeable materials for their excellent blue light transmittance [9–11] much better than those observed in inorganic crystals. The structure of the title chalcone was reported by Butcher et al., [12]. In this article, we report the synthesis, growth, characterization, and theoretical studies.

*Address correspondence to SP. Meenakshisundaram, Department of Chemistry, Annamalai University, Annamalainagar-608002, Tamilnadu, India. E-mail: meenakshisundaram.sp.294@annamalaiuniversity.ac.in, aumats2009@gmail.com

Color versions of one or more of the figures in the article can be found online at www.tandfonline.com/gmcl.

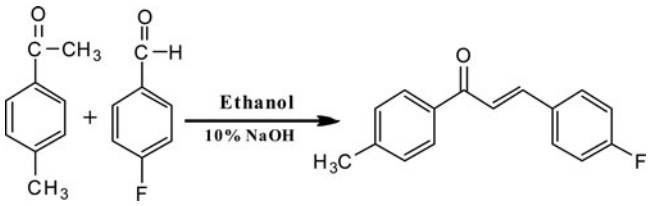

Scheme 1. Synthesis of 3-(4-Fluorophenyl)-1-(4-methylphenyl)prop-2-en-1-one (FMPP).

2. Experimental Procedure

2.1. Synthesis

FMPP was synthesized by Claisen–Schmidt condensation reaction [13]. The analytical grade starting materials, *p*-fluorobenzaldehyde (Sigma Aldrich) and *p*-methyl acetophenone (Sigma Aldrich), were used without further purification. A solution of ethanol and 10% sodium hydroxide were taken in a conical flask. A solution of *p*-fluorobenzaldehyde (0.01 mol) and *p*-methyl acetophenone (0.01 mol) dissolved in ethanol (50 ml) was prepared in a separate beaker. The aldehyde–ketone mixture was added dropwise to the conical flask with vigorous stirring (Scheme 1). During the synthesis, the temperature of the stirring solution was maintained between 20 and 25°C. After completely adding the aldehyde–ketone mixture, the solution was stirred for another 60 min. Then the reaction mixture was poured in ice cold water and neutralized with dilute hydrochloric acid. The separated product was then filtered and washed with excess of water and finally dried. The synthesized crude sample was purified by successive recrystallization from ethanol.

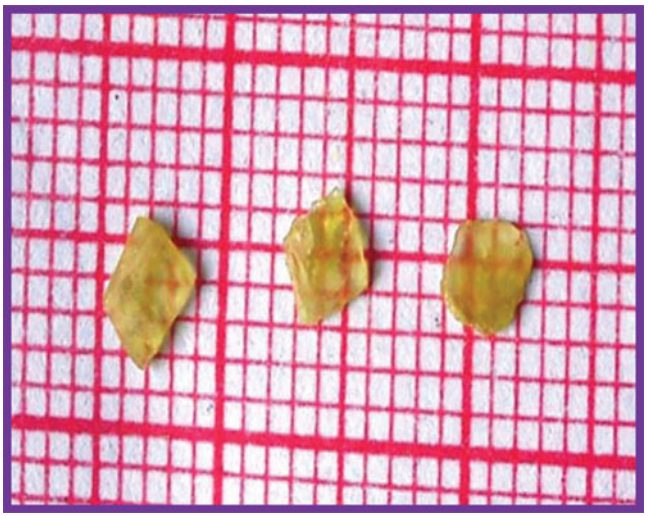

Figure 1. Photograph of as-grown FMPP crystal.

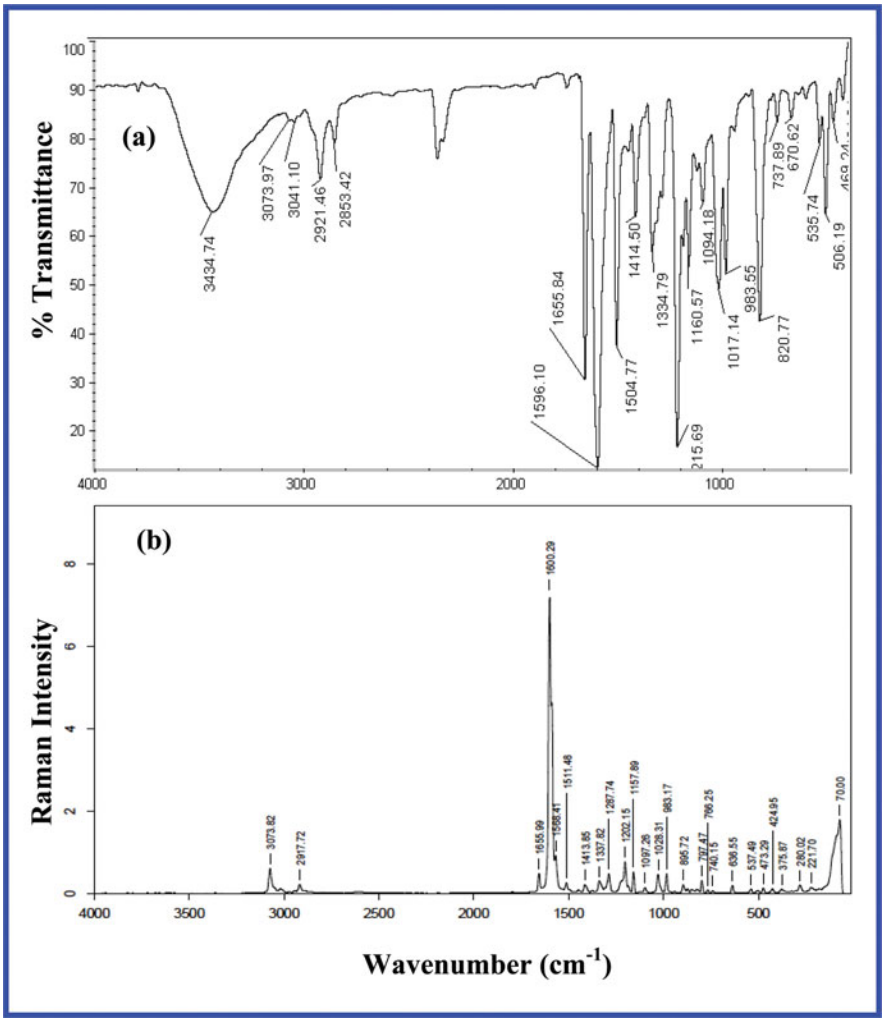

Figure 2. (a) FT-IR and (b) FT-Raman spectra of FMPP.

2.2. Crystal Growth

The crystals were grown by slow evaporation technique at room temperature. A saturated solution of FMPP was obtained by dissolving the sample in a 2:1(v/v) mixture of ethanol and chloroform with continuous stirring at room temperature. This solution was filtered using filter paper, slightly warmed and allowed to evaporate very slowly. After about 7 days, good quality transparent tiny pale yellow crystals started growing. The photograph of the as–grown crystal is shown in Fig. 1.

3. Results and Discussion

3.1. FT-IR and FT-Raman Spectroscopy

FT-IR spectrum of as-grown crystal (Fig. 2a) was recorded using AVATAR 330 FT–IR by KBr pellet technique in the spectral range of 400–4000 cm^{-1}. The sharp absorption

Table 1. Observed vibrational bands of FMPP (cm^{-1})

FT-IR	FT-Raman	Assignments of vibration
1655	1655	C=O stretching
1596	1600	alkene C=stretching
1504	1511	aromatic C=C stretching
3073	3073	aromatic C−H stretching
2921	2971	aliphatic C−H stretching
1017	1028	C−F stretching
983	983	C−H bending

band at ∼1655 cm^{-1} is due to carbonyl stretching of α,β–unsaturated carbonyl group. The medium intensity bands around ∼2921 and ∼2853 cm^{-1} are due to aliphatic C−H stretching vibrations. The sharp absorption band at ∼1017 cm^{-1} is assigned to C-F stretching vibration. The aromatic C−H stretching vibration appeared at ∼3073 cm^{-1}. The strong absorption bands at ∼1596 and ∼1504 cm^{-1} are corresponding to C=C stretching vibration. The bands observed at about 983, 820, and 737 cm^{-1} is due to aromatic C−H bending vibrations. The observed FT-IR and FT-Raman (Fig. 2b) vibrational bands are listed in Table 1.

3.2. Powder XRD

FMPP was finely powdered and subjected to powder XRD analysis using a Philips X'pert Pro Triple-axis X-ray diffractometer at room temperature using a wavelength of 1.540 Å and a step size of 0.008°. The samples were examined with Cu K_α radiation in 2θ range of 10–40°. The indexed powder XRD pattern of as-grown FMPP is shown in Fig. 3 along with simulated one. The XRD profiles show that a sample is of single-phase without detectable impurity. The well-defined Bragg's peaks at specific 2θ angles show high crystallinity of

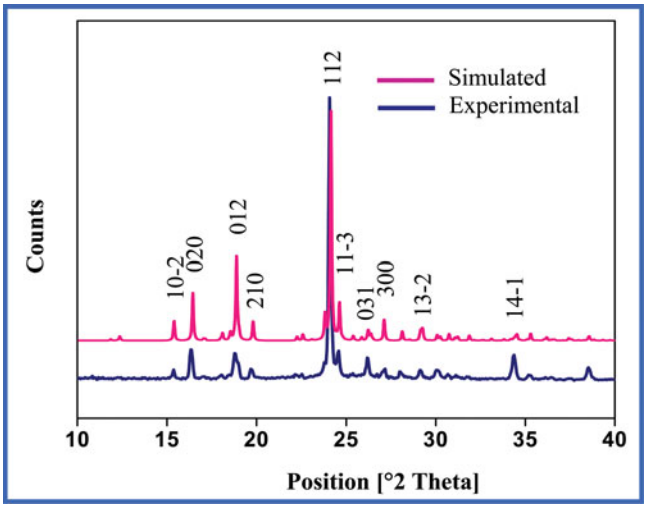

Figure 3. Powder XRD patterns of FMPP.

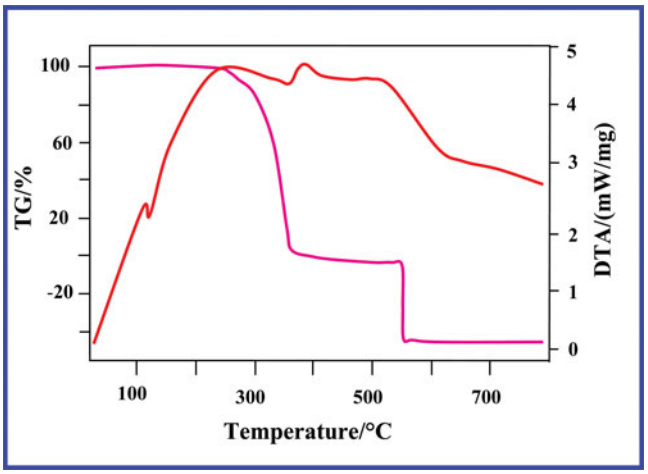

Figure 4. TG/DTA curve of FMPP.

the material. Most of the peak positions in powder XRD and simulated XRD pattern from single crystal XRD are coincide. However, the relative intensities differ. Possibly due to preferred orientations of the sample used for diffractogram measurement. Also the mosaic spread of powder and single crystal pattern may differ.

3.3. Thermal Study

In order to test the thermal stability of FMPP crystal the thermogravimetric analysis (TG) and differential thermal analysis (DTA) have been carried out simultaneously using NETZSCH STA 449F3 thermal analyzer in nitrogen atmosphere. The TG/DTA thermogram of the FMPP is shown in Fig. 4. Weight losses due to decomposition are observed at around 370°C and 550°C. An endothermic transition at 120°C indicates the melting point of the specimen and it was confirmed by using Sigma instrument (117–119°C) melting point apparatus. The absence of endo or exothermic transition below 120°C indicates the absence of the other phase transitions before the melting point of FMPP and the crystal stability. The sharpness of the endothermic peak shows good degree of crystallinity of the as-grown crystal.

3.4. SEM

The SEM images (Fig. 5) were taken at magnification values for 500× and 2000× with maximum values of 15 kV using a JEOL JSM 5610 LV scanning electron microscope. Small pores and crystal voids are observed on the surface.

3.5. Optical Studies

UV-vis spectrum of the as-grown crystal was recorded using CARY 5E UV-vis spectrophotometer. The optical reflection spectrum shows good reflectance in the visible region and the lower cut–off wavelength is ∼465 nm. The Kubelka–Munk theory [14] provides a correlation between reflectance and concentration. The concentration of an absorbing species

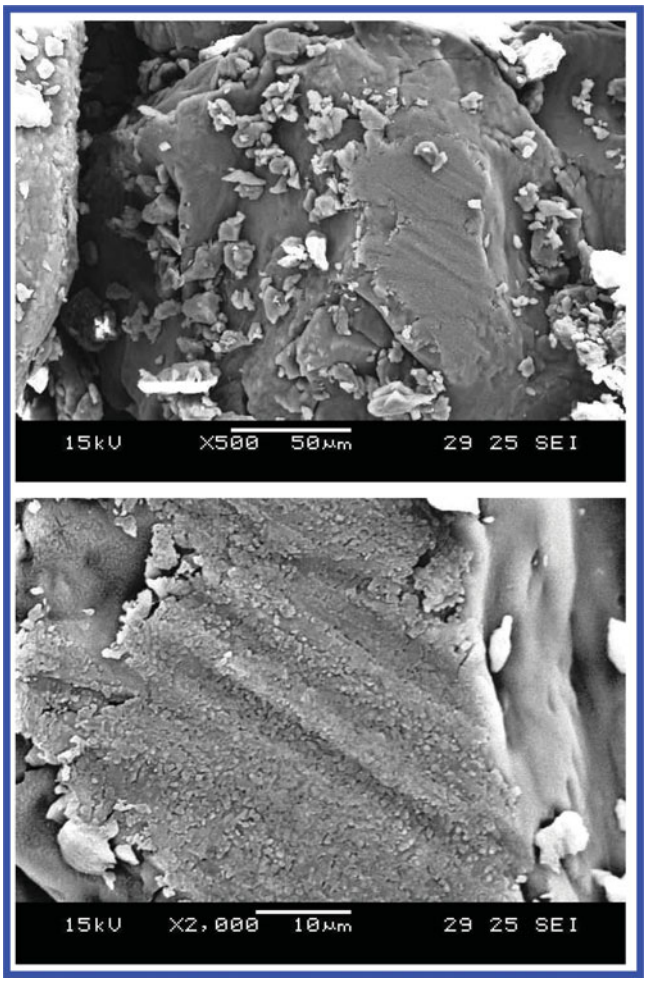

Figure 5. SEM images of FMPP.

determined using the Kubelka–Munk formula,

$$F(R) = (1 - R)^2/2R = \alpha/\mathrm{s} = \mathrm{Ac}/\mathrm{s}$$

where *F(R)* is Kubelka–Munk function, *R* is the reflectance of the crystal, *s* is scattering coefficient, *A* is the absorbance, and *c* is concentration of the absorbing species. The measurement of [*F(R)hν*] as a function of *hν* provides the band gap energy E_g of the material. The indirect band gap energy can be obtained from the intercept of the resulting straight line with the energy axis at $[F(R)\mathrm{h}\nu]^{1/2} = 0$ and the direct band gap energy from the intercept of the resulting straight line with the energy axis at $[F(R)\mathrm{h}\nu]^2 = 0$. The Tauc plots of indirect and direct band gap energies of the specimen are deduced as 2.66 and 2.85 eV, respectively, as shown in Fig. 6.

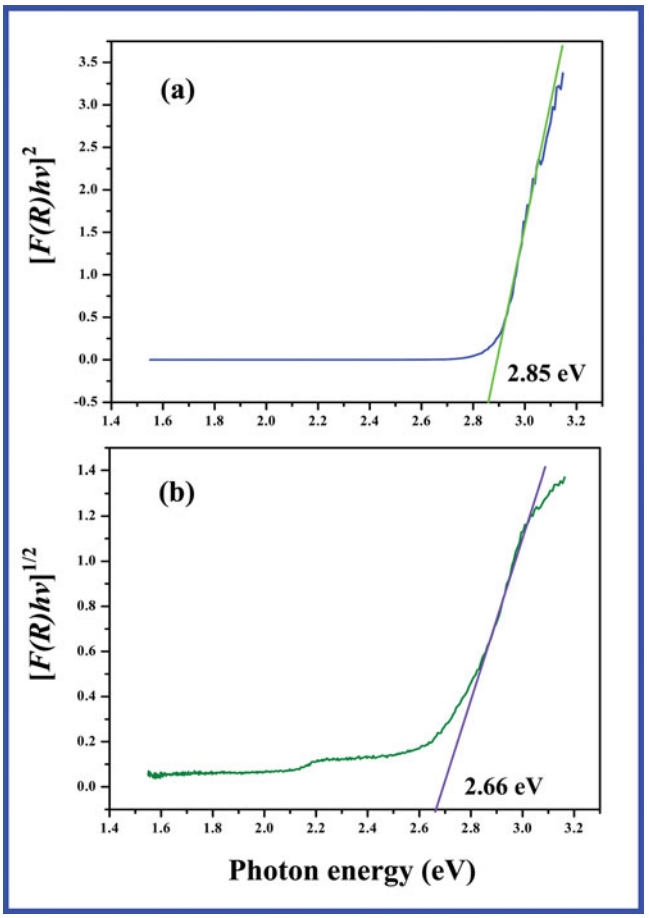

Figure 6. Tauc plot of (a) direct and (b) indirect band gap energy of FMPP.

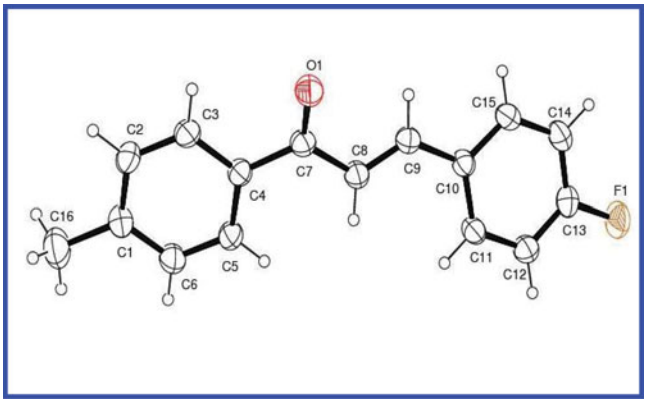

Figure 7. ORTEP diagram of FMPP.

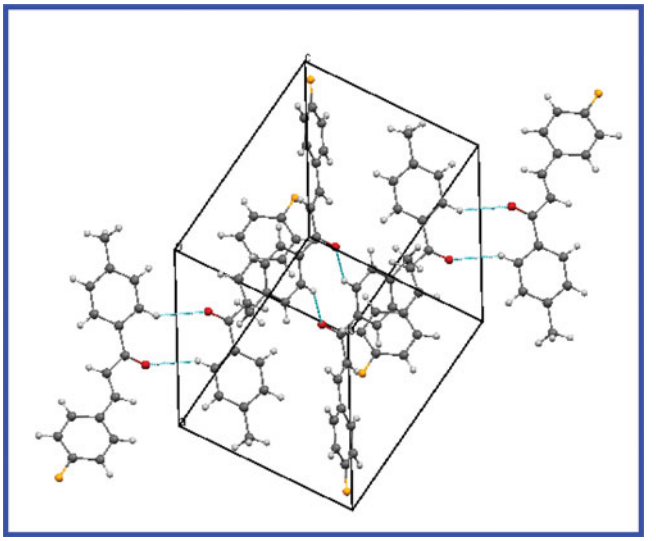

Figure 8. Packing diagram of FMPP.

Table 2. Crystal data and structure refinement for FMPP

Empirical formula	$C_{15.75}\ H_{12.25}\ Cl_{0.25}\ F\ O$
Formula weight	245.37
Temperature	293(2) K
Wavelength	0.71073Å
Crystal system, space group	Monoclinic, $P2_1/c$
Unit cell dimensions	$a = 11.010(5)$ Å, $\alpha = 90.000(5)^\circ$
	$b = 10.786(5)$ Å, $\beta = 116.460(5)^\circ$
	$c = 11.563(5)$ Å, $\gamma = 90.000(5)^\circ$
Volume	1229.3(10) Å^3
Z, calculated density	4, 1.326 Mg/m^3
Absorption coefficient	0.144 mm^{-1}
$F(000)$	512
Crystal size	0.30 × 0.20 × 0.20 mm^3
Theta range for data collection	2.07–25.00°
Limiting indices	$-13 \leq h \leq 13, -12 \leq k \leq 12, -13 \leq l \leq 13$
Reflections collected/unique	10,566 / 2157 [R(int) = 0.0254]
Completeness to theta = 22.20	99.9%
Absorption correction	Semi-empirical from equivalents
Max. and min. transmission	0.9895 and 0.9487
Refinement method	Full-matrix least-squares on F^2
Data/restraints/parameters	2157/3/167
Goodness-of-fit on F^2	1.050
Final R indices [$I > 2$ sigma(I)]	$R1 = 0.0367$, w$R2 = 0.0967$
R indices (all data)	$R1 = 0.0491$, w$R2 = 0.1069$
Largest diff. peak and hole	0.146 and −0.197 e. Å^{-3}

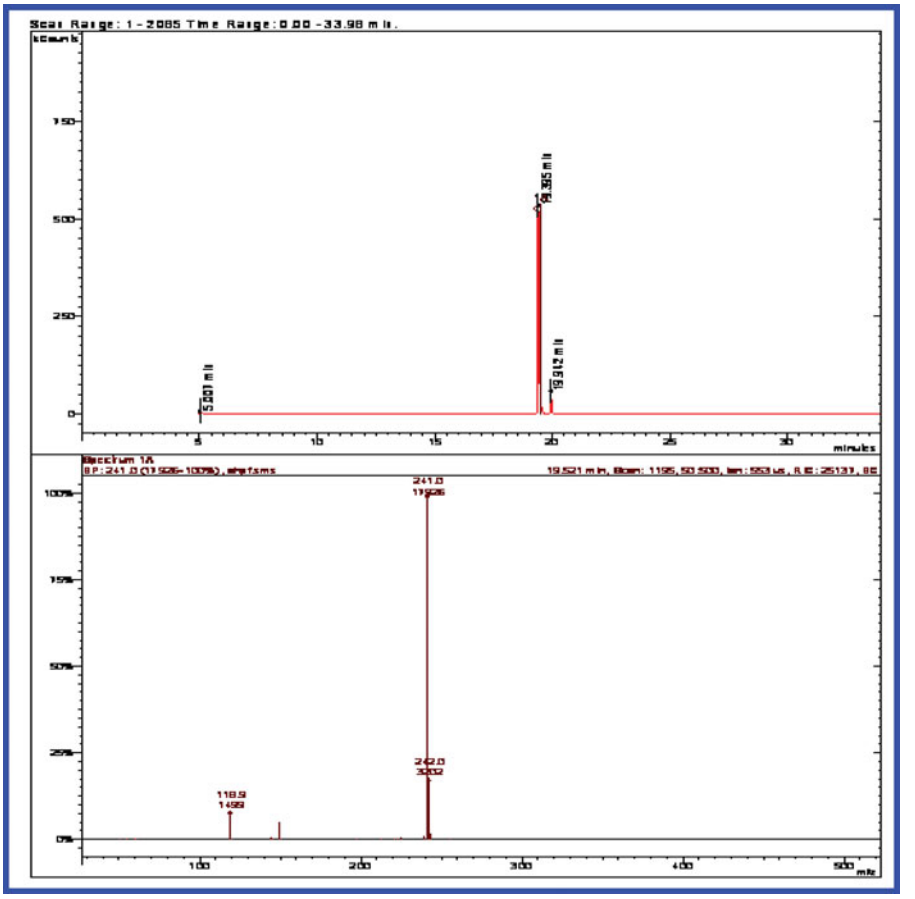

Figure 9. GC-Mass spectrum of FMPP.

3.6. Single-crystal XRD

The structural analysis of FMPP was carried out for a selected block of approximately $0.30 \times 0.20 \times 0.20$ mm^3 using Bruker AXS (Kappa APEXII) X-ray diffractometer with Mo Kα radiation ($\lambda = 0.71073$ Å). The structures were solved and refined by full matrix least squares on F^2 with WinGx software package utilizing SHELXS97 and SHELXL97 modules. It belongs to monoclinic system with centrosymmetric space group $P2_1/c$ and the cell parameters are, $a = 11.010(5)$ Å, $b = 10.786(5)$ Å, $c = 11.563(5)$ Å, $\alpha = 90.000(5)^\circ$, $\beta = 116.460(5)^\circ$, $\gamma = = 90.000(5)^\circ$, $V = 1229.3(10)$ Å^3, and $Z = 4$. These values are in close agreement with the previously reported value [12]. The ORTEP and packing diagrams are shown in Figs. 7 and 8 and the crystal data are listed in Table 2. The crystal stability and cohesion is achieved by intermolecular C-H···O hydrogen bonds.

3.7. Mass Spectrometry

Mass spectra were recorded on a VARIAN–SATURN 2000 GC–MS/MS spectrometer using electron impact technique (Fig. 9). The molecular ion peak observed at $m/z = 241$ [$(M + 1)^+$] is in good agreement with calculated molecular ion m/z = 240 (M^+) for FMPP, supported by single-crystal XRD analysis.

Table 3. The calculated dipole moment (in D), β components, β_{tot} value (in esu), α_{tot} value (in esu) and HOMO-LUMO energies (eV) of FMPP

Components	
β_{xxx}	1241.277
β_{xxy}	1180.307
β_{xyy}	−69.180
β_{yyy}	−37.828
β_{xxz}	−36.991
β_{xyz}	12.637
β_{yyz}	−18.622
β_{xzz}	26.656
β_{yxx}	−9.287
β_{zzz}	19.499
$\beta_{tot\ (x10^{-30})}$	14.254
$\alpha_{tot\ (x10^{-24})}$	28.51
μ_x	0.841
μ_y	−2.147
μ_z	0.227
μ	2.317
E_{HOMO}	−6.2612
E_{LUMO}	−2.0816
E_{HOMO} - E_{LUMO}	4.1796

3.8. Theoretical Studies

DFT calculations were performed using the Gaussian 09 W [15] program package on a personal computer without any constraints on the geometry using 6-31G(d,p) as the basis set [16]. By the use of the Gaussview 5.0 molecular visualization program [17], the optimized structure of the molecule has been visualized.

The calculated polarizability (α), first-order molecular hyperpolarizability (β), and dipole moment (μ) of the specimen are 28.51 × 10^{-24} esu, 14.254 × 10^{-30} esu (~43 times

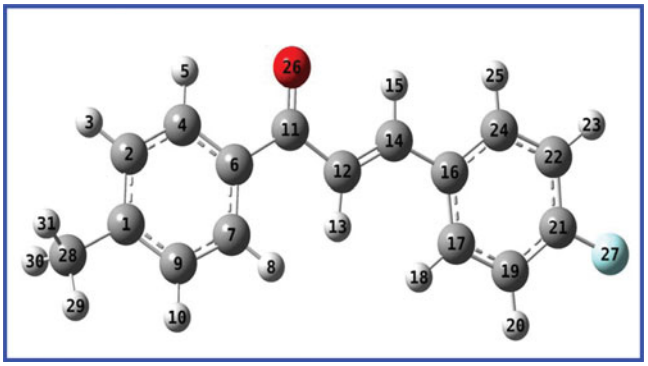

Figure 10. Optimized molecular structure of FMPP.

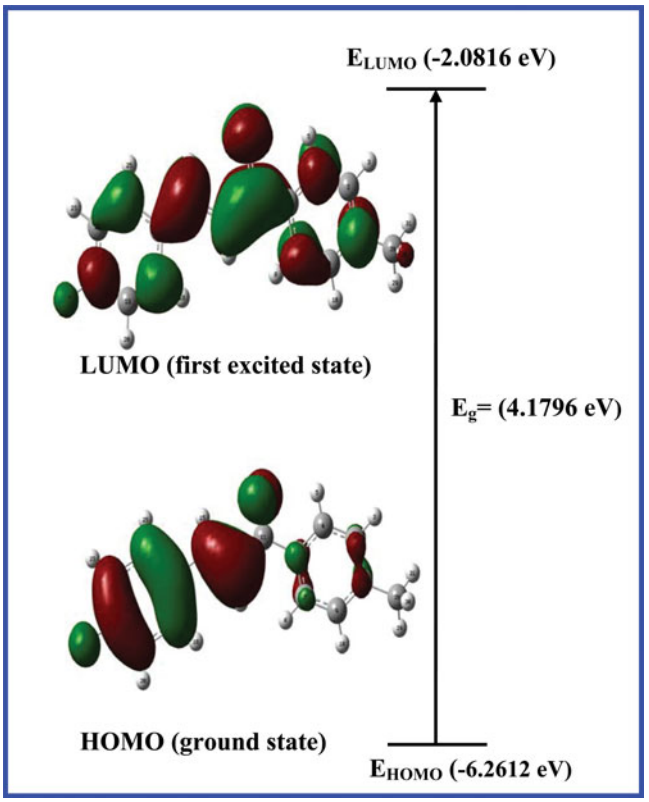

Figure 11. Frontier molecular orbital diagram of FMPP.

of urea), 2.3173 D, respectively (Table 3). The maximum β is due to the behavior of nonzero μ values. The optimized molecular structure of FMPP (Fig. 10) closely resembles the displacement ellipsoid diagram (Fig. 7). High β is associated with high charge transfer.

Figure 11 shows the highest occupied molecular orbital (HOMO) and lowest unoccupied molecular orbital (LUMO) of FMPP. The frontier orbital gap facilitates in characterizing the chemical reactivity and kinetic stability of the molecule. The red and green colors represent the positive and negative values for the wave function. The HOMO is the orbital that primarily acts as an electron donor and the LUMO is the orbital that mainly acts as an electron acceptor.

4. Conclusions

Transparent tiny crystals of 3-(4-fluorophenyl)-1-(4-methylphenyl)prop-2-en-1-one were grown in ethanol and chloroform 2:1(v/v) by the slow evaporation solution growth technique at room temperature. The product formation was confirmed by FT–IR, FT–Raman, GC–Mass, and single-crystal XRD analyses. The crystallographic data indicate that the FMPP crystallizes in monoclinic system with centrosymmetric space group of $P2_1/c$ .The powder X-ray diffraction study shows the good crystallinity of the material. TG/DTA study reveals the purity of the sample and no decomposition is observed up to the melting point. Good transmission in the visible region is observed and the direct and indirect band

gap energy is estimated as 2.85 and 2.66 eV, using the reflectance data. Molecular level nonlinearity with high first-order molecular hyperpolarizability is observed.

Funding

The authors thank the Council of Scientific and Industrial Research (CSIR), New Delhi, for financial support through research grant No.03(1233)/12/EMR-II, and V.M is grateful to CSIR project for the award of Senior Research Fellowship (SRF). K.M is thankful to CSIR, New Delhi, for the award of SRF.

References

[1] Nielsen, S. F., Christensen, S. B., Cruziani, G., Kharazmi, A., & Liljefors, T. (1998). *J. Med. Chem.*, *41*, 4819–4832.
[2] Liu, M., Wilairat, P., & Go, M. L. (2001). *J. Med. Chem.*, *44*, 4443–4452.
[3] Rojas, J., *et al.* (2002). *Eur. J. Med. Chem.*, *37*, 699–755.
[4] Calvino, V., Picallo, M., Lopez-Peinado, A. J., Martın-Aranda, R. M., & Duran-Valle, C. J. (2006). *Appl. Surf. Sci.*, *252*, 6071–6074.
[5] Chemla, D. S. (1987). *J. Zyss*, Academic Press: New York.
[6] Prasad, P. N., & Williams, D. J. (1991). Wiley: New York.
[7] Oudar, J. L., & Chemla, D. S. (1977). *J. Chem. Phys.*, *66*, 2664–2668.
[8] Oudar, J. L. (1977). *J. Chem. Phys.*, *67*, 446–457.
[9] Zhao, B., Lu, W. Q., Zhou, Z. H., & Wu, Y. (2000). *J. Mater. Chem.*, *10*, 1513–1515.
[10] Fichou, D. *et al.* (1988). *Jpn. J. Appl. Phys.*, *27*, L429–L434.
[11] Goto, Y., Hayashi, A., Kimura, Y., & Nakayama, M. (1991). *J. Cryst. Growth.*, *108*, 688–698.
[12] Butcher, R. J., Jasinski, J. P., Yathirajan, H. S., Narayana, B., & Veena, K. (2007). *Acta Cryst.*, *E63*, o3833.
[13] Vogel, A. I. (1989). *Practical Organic Chemistry. 5th ed.*
[14] Kubelka, P., & Munk, F. (1931). *Z. Tech. Phys.*, *12*, 593–595.
[15] Frisch, M. J., *et al.* (2009). Gaussian 09, Revision D.01, Gaussian, Inc.,Wallingford CT.
[16] Schlegel, H. B. (1982). *J. Comput. Chem.*, *3*, 214–218.
[17] Frisch, A., Nielson, A. B., Holder, A. J., (2000). *Gaussview User Manual*, Gaussian Inc.: Pittsburgh, PA.